High Density Laser Wakefield Acceleration

Senior Thesis (Spring, 2021)

Carlton Kim
University of California at Irvine

Senior Thesis Advisor: Professor Toshiki Tajima
Department of Physics and Astronomy

Abstract

Laser wakefield acceleration (LWFA) utilizes the collective force of plasma induced by short laser pulses. This paper focuses on studying the seldom studied high plasma density regime of LWFA. We study this new regime via the particle-in-cell method - specifically, the code EPOCH. In addition to the high density focus, we explore the regime of weak to moderate laser intensity. We find that in the weak to moderate intensity regime, the electron maximum enemies are higher than the well known LWFA energy gain expression that applies to the low density regime (with moderate to high laser intensity) which predicts energy gain falling as the plasma density approaches the critical density. We explore this phenomena and examine where well-developed LWFA expectations break down and where it can, in fact, support our findings.

Table of Contents

List of Figures

Chapter 1 - Background and Introduction

I. Introduction

Laser Wakefield Acceleration (LWFA) [1] is a compact method to accelerate charged particles to high energies that was first proposed by Tajima and Dawson [2] in 1979. While the accelerating electric field in a conventional linear accelerator is limited by the breakdown threshold of the device walls, plasma-based accelerators can access far higher electric fields, owing to the inherently broken-down nature of plasma. Consequently, plasma-based accelerators can access far higher accelerating gradients than those available to conventional accelerators, reaching potentially GeV per cm or higher. The original proposal for LWFA called for a laser intensity of 10^{18} W/cm^2 , but this regime of intensity only became accessible after the invention of Chirped Pulse Amplification (CPA) [5], and LWFA was experimentally verified shortly thereafter [4, 5]. Since then, many more experiments demonstrated this technique in different regimes, and the field has grown steadily. Accelerators have many applications in our current society, one of the most important being their use in radiation therapy. Particle beams in the form of X-rays, electrons, and protons can be used to treat cancer. These energetic beams can ionize molecules which in turn damage cellular DNA. Cells with damaged DNA can not reproduce and are eliminated through natural processes in the body. The type of beam used depends highly on the size and location of cancer being treated. For example, while X-rays and electrons deposit most of their energy in the surface layers, protons can be controlled to deposit their energy at a specific depth due to Bragg peak phenomena [6, 7], dramatically reducing damage to healthy cells. Proton therapy contends with other limitations, however [8].

Current accelerators used for radiation therapy use traditional linear accelerator technology. To produce an electron or X-ray beam, electrons from an electron gun are accelerated and guided through waveguides using electric fields and magnets. These electrons can eventually hit a target and produce X-rays. However, the material breakdown limits of linear accelerators tend to require that these machines be large and costly. The typical electron energy needed for radiation therapy is between 5-20 MeV. LWFA techniques can accelerate electrons to these energies in micron to millimeter scale lengths. Such a high acceleration gradient reduces the size and cost of these machines, consequently increasing their availability. Research in the use of LWFA to generate electron beams for medical applications has proceeded for more than

two decades now. Initially, these efforts focused on the generation of high-quality electron beams with energies roughly in the range 6-25 MeV, as would be applicable for conventional, external sources of radiation for cancer therapy [9–15]. Recent innovations in the field of fiber lasers has offered a new leap forward in this effort: the Coherent Amplification Network (CAN) [16], in which many individual micron-scale fiber lasers are coherently combined and amplified to provide both high-rep rate and high power. In such a scheme, laser accelerators could possibly be further compactified to be viable even for endoscopic applications. If electrons can be generated inside of a patient's body (or in an intraoperative [12, 13] fashion), the desired energy of these accelerated electrons (and X-rays converted from them) is much lower than those of typical, high-energy LWFA (MeV and above), as they need not traverse healthy tissues before reaching the tissues to be treated. Consequently, we wish to study LWFA in the high-density, low intensity regime. This regime has been less explored in detail than that of the more typical, low-density, high energy regime of LWFA. Subsequently we focus on this regime with intended applicability to fiber lasers, emphasizing the fundamental physics and taking only the beginning steps towards medical applications. Prior work [17] focuses more explicitly on medical applications.

Even at very modest intensity, LWFA can produce electrons that are relevant for tissue penetration and delivery of beams of ionizing radiation. With this insight, in combination with the compactness afforded by the recent developments in fiber lasers, we are led to consider the new situation of in situ radiation sources (of electrons). In this vision, we see three chief schemes in which the wakefield electron source could be brought directly to the cancer. First, the laser-wakefield accelerator could be inserted in an intraoperative fashion, [10,11] which involves surgically opening the intervening tissues and can presently be used for LINAC sources in some instances. A surgeon may also use such an operation to remove any residual cancer or clean affected tissues by hand. Less invasive is brachytherapy, where the laser is injected discreetly into the body, such as through a blood vessel or directly through tissue. Finally, it may be possible to carry the laser into the body in an endoscope, whereby the surgeon could potentially both diagnose and treat the cancer simultaneously. It is our goal here to devise a way in which any or all of these methods might be possible with LWFA. In each of these cases, the electrons beam need only have shallow penetrative power, as they need not traverse the body before

reaching the tissues to be treated. The desirable energy for an electron beam then reduces to the order of 10^2 keV. We thus seek a means of producing low-energy electrons.

II. Physics of Laser Wakefield Acceleration

The electron energy gain from LWFA is given by:

$$\Delta E = 2g(a_0)m_ec^2(n_c/n_e)$$

$a_0 = eE_0/m_e\omega_l c$ = normalized vector potential of the laser pulse

E_0 = Electric field of laser

$g(a_0)$ represents the function dependence of energy gain on a_0 and is generally taken to be unity at $a_0 = 1$. n_c is the laser critical density, and n_e is the plasma density [3]. The critical density is derived from the dispersion relation of a plasma, $\omega^2 = \omega_p^2+c^2k^2$, where k is wavenumber of the laser. At the critical density, the frequency of the plasma and the laser match, as there is no propagation of the laser into the plasma (k=0). Substituting ω_p with its equation leads to:

$$\omega^2 = \frac{n_c e^2}{\epsilon_0 m}$$

$n_c = \varepsilon_0 m\omega^2/e^2$.

The energy gain relation suggests a path to low-energy electrons through a high plasma density and modest laser intensity - parameters that are also favorable to fiber lasers. To provide a target material near the critical density of an optical laser (n_c = 1.11*10^21 cm^{-3} for a laser wavelength of 1 micron), it may be best to use a porous nanomaterial [15-17], such as porous alumina or carbon nanotube. Such a target material for irradiation by the laser would also avoid the presence of ionized gas inside the body.

While the low-density, high-energy regime of LWFA has been studied extensively, the high-density, low-energy regime has been less explored in detail [18]. Indeed, the expression for electron energy gain given above was established by studying the low-density regime. As a foundation for these applications, the physics of the high-density regime of LWFA has been recently studied in Nicks et al., 2019 [19]. This work studied first the scaling laws of the electron energy gain for n_c/n_e and a_0. It was found that $\Delta E \propto n_c/n_e$, the proportionality predicted by low-density wakefield theory, was obeyed in the regime $n_c/n_e \gtrsim 1$ for the highest-energy electrons. Next, the mechanics of electron acceleration in the regime $n_c/n_e \sim 1$ were studied, revealing sheath acceleration [20] that generates a peculiar

stream-like distribution of bulk electrons in phase space. This bulk acceleration by sheath contrasted significantly with the trapping and acceleration seen in low-density wakefield. This work then attempted to quantitatively distinguish this high-density, sheath regime from the more typical wakefield physics seen at low densities. Finally, this work briefly examined the penetrative power of such an accelerated spectrum of electrons in water, approximating biological tissue.

III. High Density Regime Acceleration

The interaction of the laser with the plasma in the two contrasting regimes of high and low density has a convenient analogy in tsunami waves in a certain property of the wave dynamics. The phase velocity of the wake field matches the laser group velocity in the plasma ($v_g = c(1-n_e/n_c)^{1/2}$ much as sea-floor depth determines the phase velocity of an ocean wave. The deep water of the open ocean allows tsunami waves to propagate with a fast phase velocity given by $v_{ph} = p$ g/k with wavenumber k [22], where g is the constant of gravitational acceleration. This fast phase velocity causes only weak interaction with stationary objects (such as boats). Near the shore, however, the shallow water forces the wave to move with a slower phase velocity given by $v_{ph} = \sqrt{gh}$, where h is the water depth. As its phase velocity slows, the wave steepens and amplifies until breaking occurs. Two key related consequences follow. First, the slow phase velocity causes strong and catastrophic coupling to stationary objects. Second, the turbulent process of wave breaking causes dredging of sediment from the seabed. The sediment is then incorporated into the wave and transported forwards, creating a visibly black wave. The momentum transport imparted to the sediment can be considered to represent an effective viscosity caused by the turbulence of wake breaking. In contrast, the wave in the open ocean does not incorporate sediment and thus remains blue.In the open ocean, where the water depth is great, tsunami waves propagate with a fast phase velocity and thus do not couple to stationary objects. Boats in the ocean, for instance, may move slightly in the transverse direction (vertically), but are

not otherwise affected. The waves in this regime also do not couple to the sediment on the seafloor, and so remain "blue". An object such as a surfer could only be trapped and accelerated by these waves by exerting a great deal of effort to approach the wave phase velocity. So it is with wakefield: in the low-density regime, the wake phase velocity is near the speed of light, and while a small number of elections may be accelerated to high energies, the wake does not couple to the bulk motion of the plasma. The wake and accelerated electrons form a clean and coherent train. Near the shore, however, the increasingly shallow water causes the phase velocity of the wave to slow down, which leads to amplification and steepening of the wave until breaking occurs. The slow velocity of the wave near the shore then causes catastrophic "trapping" of stationary objects. Additionally the slow wave velocity couples with turbulence created by wave breaking to create anomalous transport on the sediment bed. Significant amounts of sediment quickly pass into the wave, creating a visibly "black" tsunami from the clean, "blue", off-shore starting wave and leading to momentum transport of the sediment. Similar physics occurs in wakefields near the critical density. The laser couples strongly to the bulk motion of the plasma, creating a qualitatively distinct regime that features sheath acceleration and bulk flow of electrons. The typical approach to LWFA, which seeks to generate high-energy electrons, is to use a low-density plasma ($n_c/n_e>1$). In this regime, which we may call the "blue wave" case ($v_g \cong c$), a train of coherent wake waves follows the laser pulse. This wake then accelerates a regular train of electrons. The wakefield, which is a longitudinal electric field, reaches a saturation value on the order

of the TajimaDawson field [5,26]: $E_{TD} = m_e \omega_p c/e$, where ω_p is the plasma frequency. This state of affairs reigns until the laser has traveled either the dephasing length, at which electrons begin to decelerate, or the pump depletion length, at which the laser has lost significant energy to the plasma and can no longer excite a robust wakefield. The high group velocity of the laser leaves the bulk plasma intact and creates a "blue" wakefield. In contrast, the case of $n_e = n_c$, the "black wave", exhibits quite different behavior. Here, $v_g = 0$, restricting the laser-plasma interaction to within one plasma wavelength. The long train of trapped electrons in the low-density case becomes replaced by streams of low-energy (E ~ 100 keV) electrons ejected from the site of laser entry roughly every plasma period. These electrons are accelerated by an oscillating sheath that is formed by the laser at the initial boundary of the domain. This behavior is somewhat reminiscent of laser interaction with a solid target and previous sheath acceleration efforts. However, some diminished part of the laser is still able to propagate through the target, and the ions have essentially no response. The "blackness" of the wave derives from its strong coupling to the bulk electrons, which occurs because $v_g = 0$ for the laser, much as an ocean wave that slows down near the shore becomes turbulent and dredges sediment from the sea-floor. As ne is decreased from the critical density, a transition between the "black" and "blue" regimes is seen - the "grey" case which shows elements of the bulk flow of high-density wakefield as well as elements of more typical, low-density wakefield. These sheath mechanics may also be useful for the understanding of related ion acceleration dynamics.

IV. Beat Wave Acceleration

Another approach using practical fiber laser parameters is the laser beat-wave accelerator, 3,34 which was used historically in the early years of LWFA. In this scheme, two lasers with frequencies differing by ωp create a modulation at the plasma frequency and resonantly excite the wakefield. Exploration of this possibility at $n_c/n_e = 10$ with a 100 fs Gaussian pulse and 15 $a_0 = 0.01$ lasers, each divided into two equal components separated in frequency by ωp, done by Nicks et. al.,2019 [19] , yielded slightly more efficient acceleration, with electrons reaching energies slightly in excess of 1 MeV. This relatively clean acceleration is expected given the seeded plasma oscillation and provides a confirmation of the physics of the pre-

modulated laser field. As in the self-modulating case, here a lower laser harmonic equivalent to $n_c/n_e = 4$ is used, as well as harmonics higher than the nominal frequency, the former perhaps aiding bulk acceleration of electrons and the latter pulling the highest-energy electrons past the energies reached in self-modulated case. In these examples, an initially "blue" wave is converted into a "black" wave that can efficiently accelerate low-energy electrons even at very low laser intensity. Together with a variable number of coherently added fibers, this effect may provide substantial practical flexibility for a medical fiber laser application. For instance, if an optimized setup required an even lower individual laser intensity than 10^{14} W/cm^2, the target density could be modestly lowered, preserving the bulk flow of electrons in the desired energy range. Furthermore, if a beat-wave laser is possible, a potentially cleaner electron beam can also be produced if desired. It is remarkable that these benefits derive from the requirement of a long laser pulse, which is in fact considered one of the "limitations"of fiber lasers.

Chapter 2 - Simulation of Beat Wave Acceleration

I. Particle in Cell

To develop intuition and understanding of the low intensity, high density regime, this work refers to simulations using the particle-in-cell code EPOCH. Particle-in-cell simulates plasma by calculating certain characteristics of the plasma within a discrete grid, leading to simulated pseudoparticles rather than individual particles. The code begins by using equations of motion to determine the position and velocity of the particles using the old values relative to the grid. The code then solves Maxwell's equations using the positions of these pseudoparticles

relative to the defined grid. By solving for their fields, the forces which on particles a suitable distance from a grid point can be found. The subsequent position of the particles can then be determined, and the same iterative cycle can resume.

II. High Density Beat Wave Acceleration Simulation

In EPOCH, the plasma parameters were adjusted to monitor densities in both the "gray" regime and the "black" regime by altering the density from 10^{20} particles/cm^3 to 10^{21} particles/cm^3 in 10^{20} increments.

For a beat wave to excite a target plasma, the beat wave was set such that the beat frequency, ω_{beat}, matches the plasma frequency. Therefore:

$$\omega_p = |\omega_{L1} - \omega_{L2}|$$

where ω_{L1} corresponds to a 1.05 micron laser in each case, whereas the second laser has a varying wavelength to fulfill the resonating condition of the beat and plasma frequencies matching. To build upon previous works, the normalized phase space of the plasma was analyzed first with a_0=1.

A. Low-Intensity Laser

After verifying the phase space properly reflects the physics of high density wakefield phenomena, the energy distributions of the plasma at each density were examined. At the a_0 values of 0.03 and 0.1 in Fig. 1, the maximum energy values depart from the max energy values of typical LWFA, where $\Delta E \propto n_c/n_e$. In these cases the energy tends to increase as the electron density increases toward the critical density. LWFA theory predicts that the energy with a_0=0.03 and n_e/n_c=0.2 is 2.25 keV, which is larger than the resultant maximum energy by a factor of ~2. For the a_0=0.1 case when n_e/n_c=0.2, the prediction is instead an underestimation, where the energy is expected as 0.25 MeV. Based on this disagreement, it seems that the departure from the typical conditions of wakefield acceleration creates sharp distinctions in predictions.

Additionally, the typical theory predicts the maximum energy to decrease as the plasma density increases. However, as shown in Fig 1, the maximum energy increases with density in both the a_0=0.03 and 0.1 case.

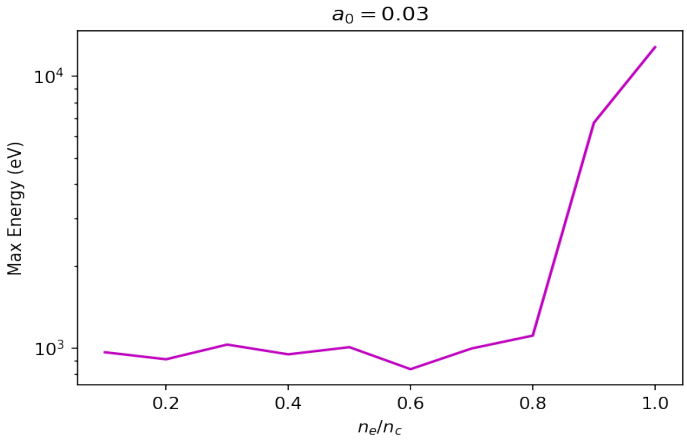

Fig 1 - Maximum energy plotted over the density ratio from a low to high density in the low intensity regime shows the breakdown of conventional LWFA prediction of the energy's inverse relationship with n_e.

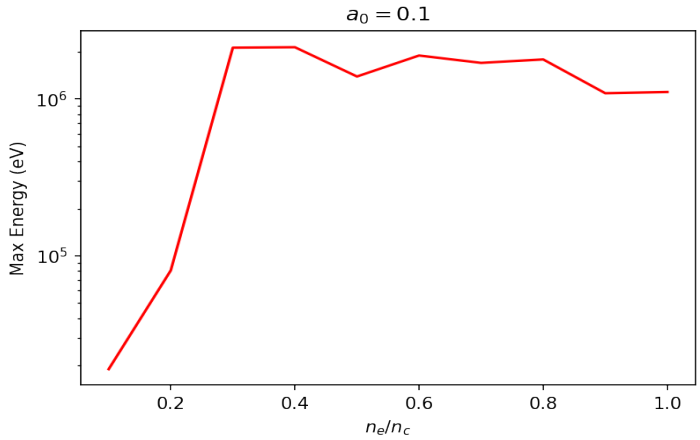

Fig 2 - At a slightly higher intensity compared to a_0=0.03, the maximum energy retains the same trend of increasing as density approaches the critical density.

The energy distribution graphs for the a_0=0.03 case were plotted and examined to monitor how such a low intensity laser would affect the electrons in the target plasma. Figure 2 shows the energy distribution functions for varying density plasmas.

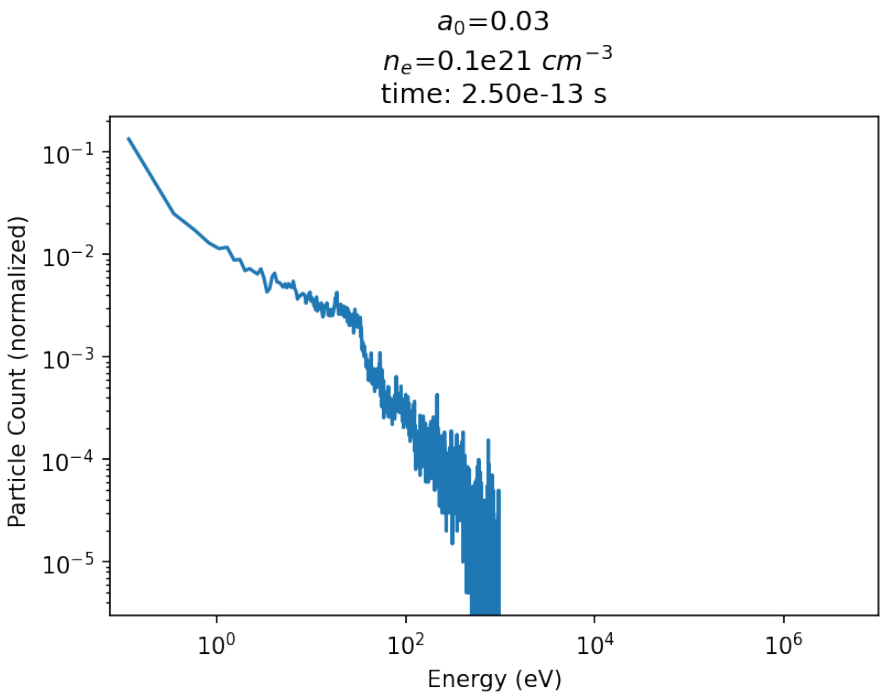
a_0=0.03
n_e=0.1e21 cm^{-3}
time: 2.50e-13 s
Particle Count (normalized)
10^{-1}
10^{-2}
10^{-3}
10^{-4}
10^{-5}
10^0
10^2
10^4
10^6
Energy (eV)

(a)

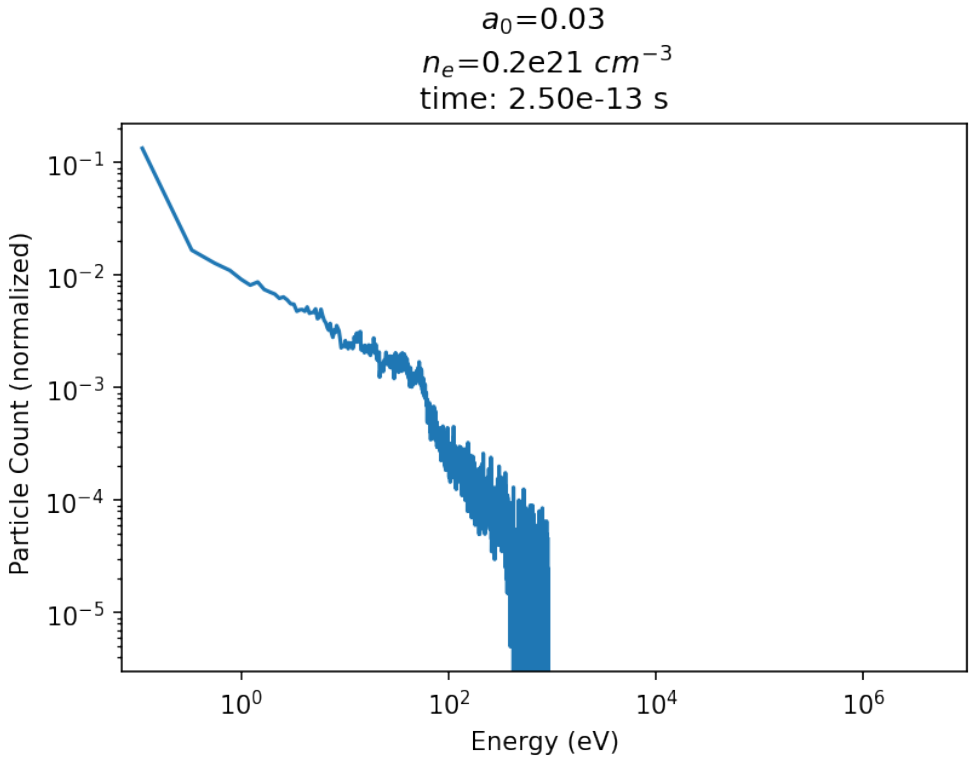
a_0=0.03
n_e=0.2e21 cm^{-3}
time: 2.50e-13 s
Particle Count (normalized)
10^{-1}
10^{-2}
10^{-3}
10^{-4}
10^{-5}
10^0
10^2
10^4
10^6
Energy (eV)

(b)

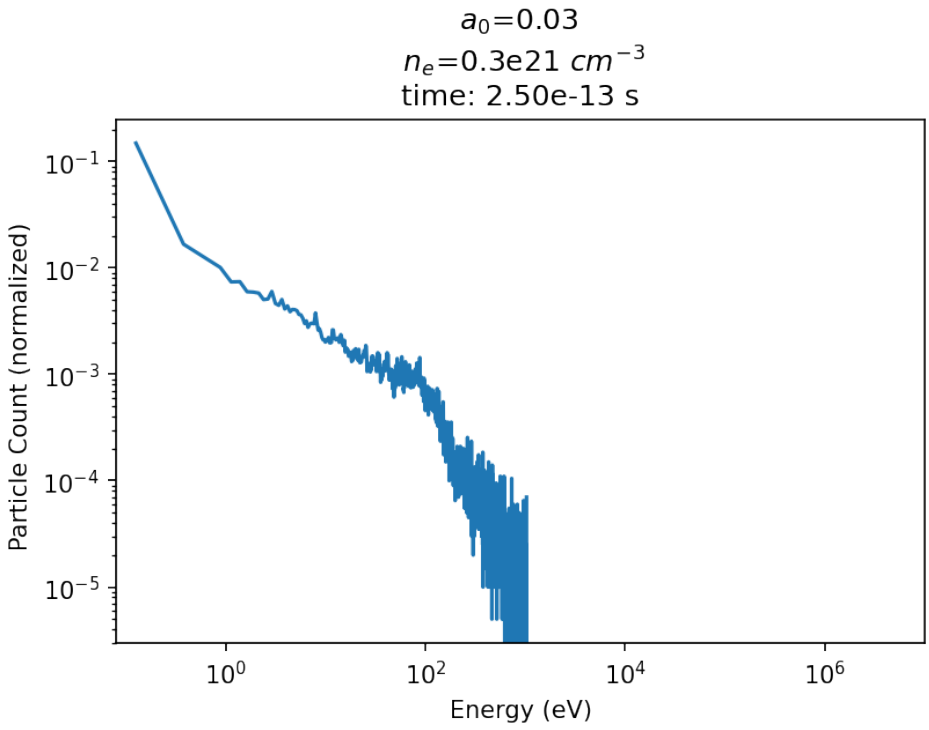
a_0=0.03
n_e=0.3e21 cm^{-3}
time: 2.50e-13 s
Particle Count (normalized)
10^{-1}
10^{-2}
10^{-3}
10^{-4}
10^{-5}
10^0
10^2
10^4
10^6
Energy (eV)

(c)

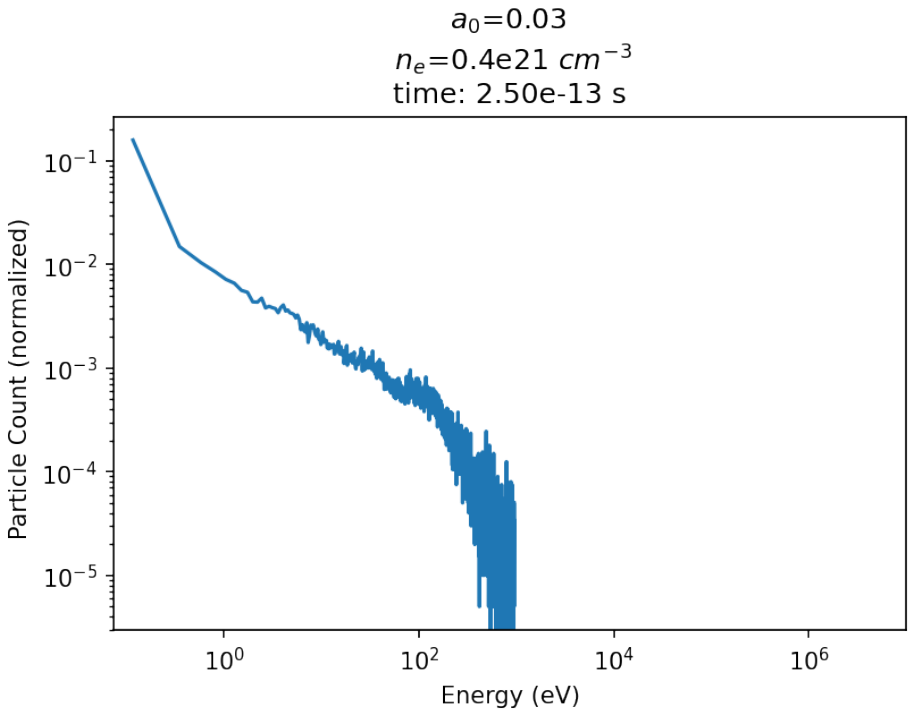
a_0=0.03
n_e=0.4e21 cm^{-3}
time: 2.50e-13 s
Particle Count (normalized)
10^{-1}
10^{-2}
10^{-3}
10^{-4}
10^{-5}
10^0
10^2
10^4
10^6
Energy (eV)

(d)

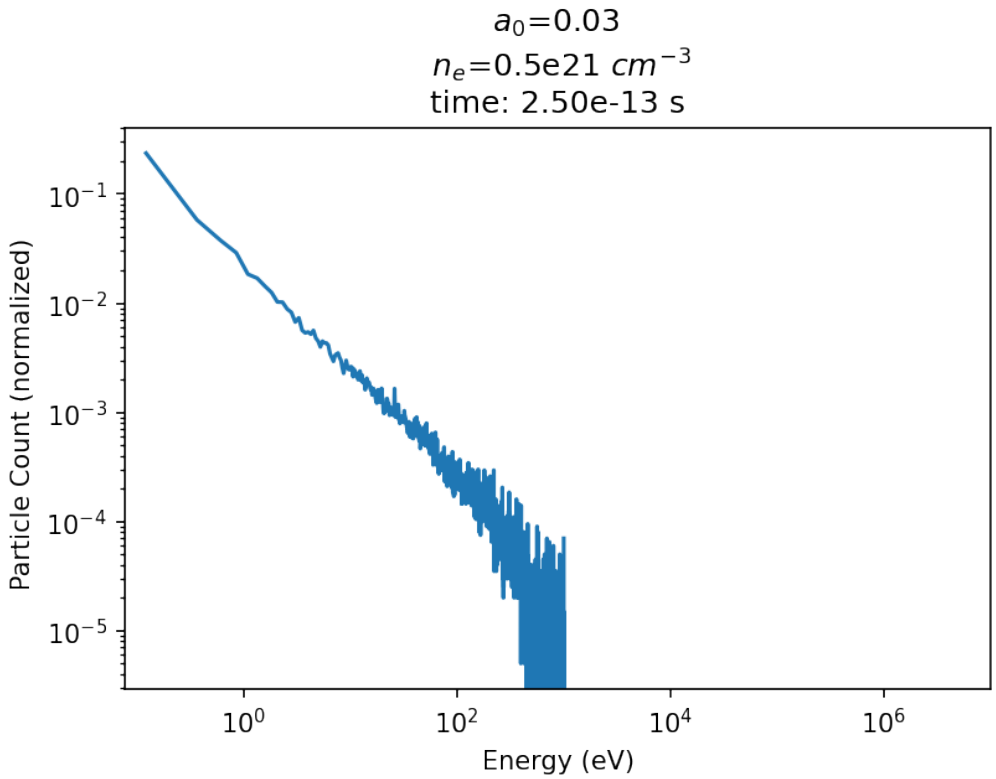
a_0=0.03
n_e=0.5e21 cm^{-3}
time: 2.50e-13 s
Particle Count (normalized)
10^{-1}
10^{-2}
10^{-3}
10^{-4}
10^{-5}
10^0
10^2
10^4
10^6
Energy (eV)

(e)

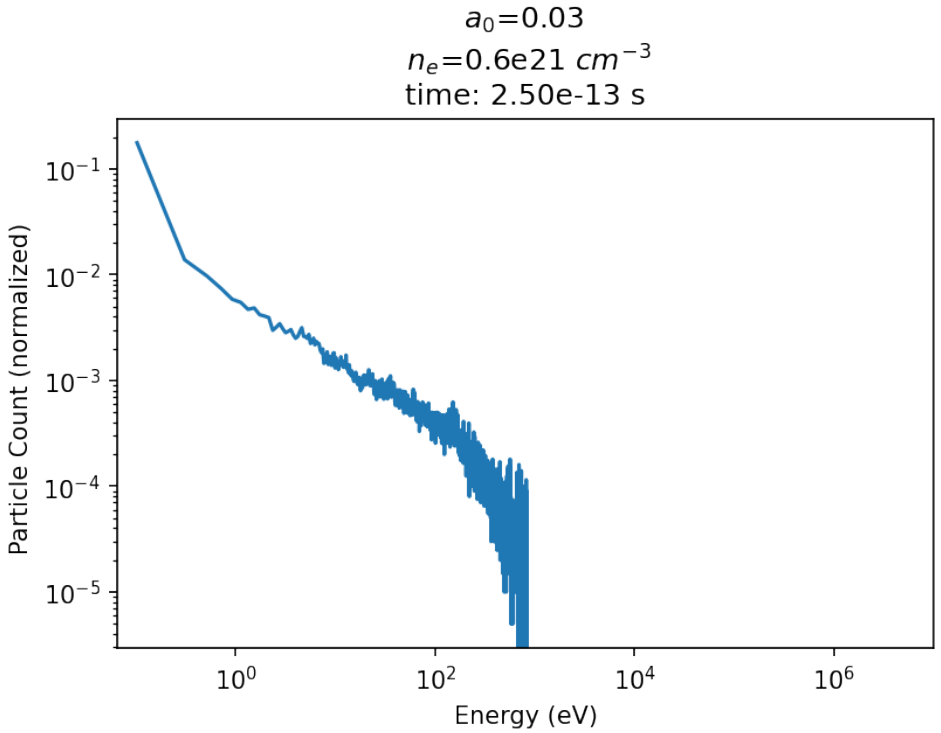
a_0=0.03
n_e=0.6e21 cm^{-3}
time: 2.50e-13 s
Particle Count (normalized)
10^{-1}
10^{-2}
10^{-3}
10^{-4}
10^{-5}
10^0
10^2
10^4
10^6
Energy (eV)

(f)

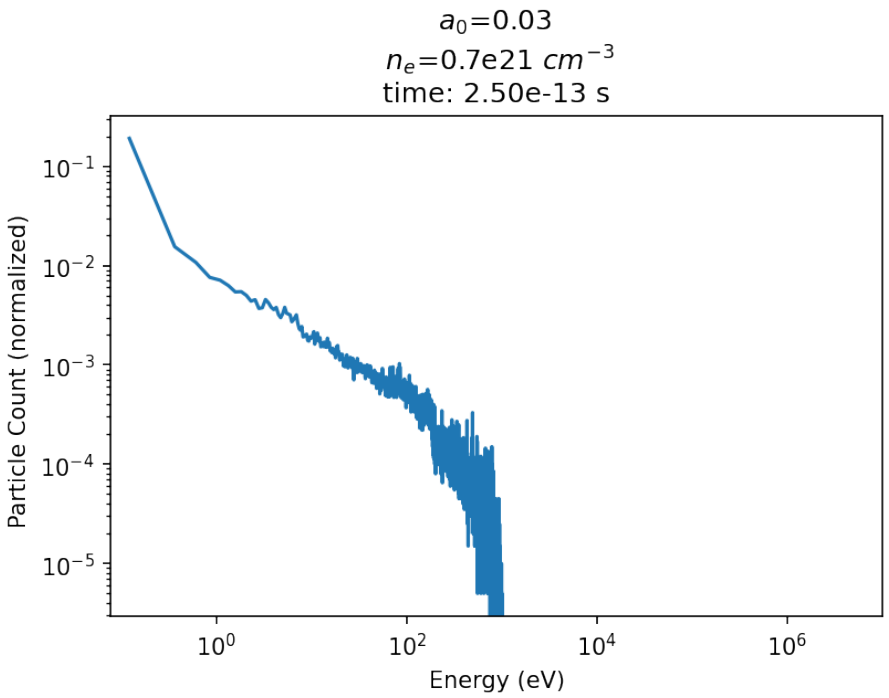
a_0=0.03
n_e=0.7e21 cm^{-3}
time: 2.50e-13 s
Particle Count (normalized)
10^{-1}
10^{-2}
10^{-3}
10^{-4}
10^{-5}
10^0
10^2
10^4
10^6
Energy (eV)

(g)

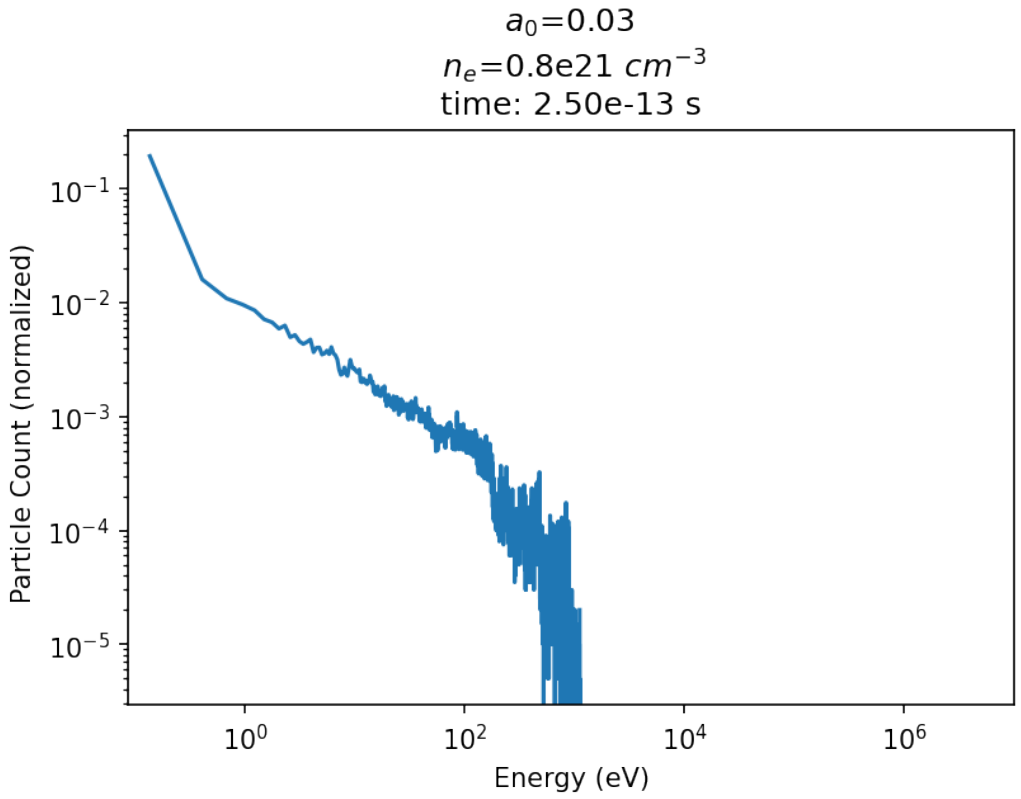
a_0=0.03
n_e=0.8e21 cm^{-3}
time: 2.50e-13 s
Particle Count (normalized)
10^{-1}
10^{-2}
10^{-3}
10^{-4}
10^{-5}
10^0
10^2
10^4
10^6
Energy (eV)

(h)

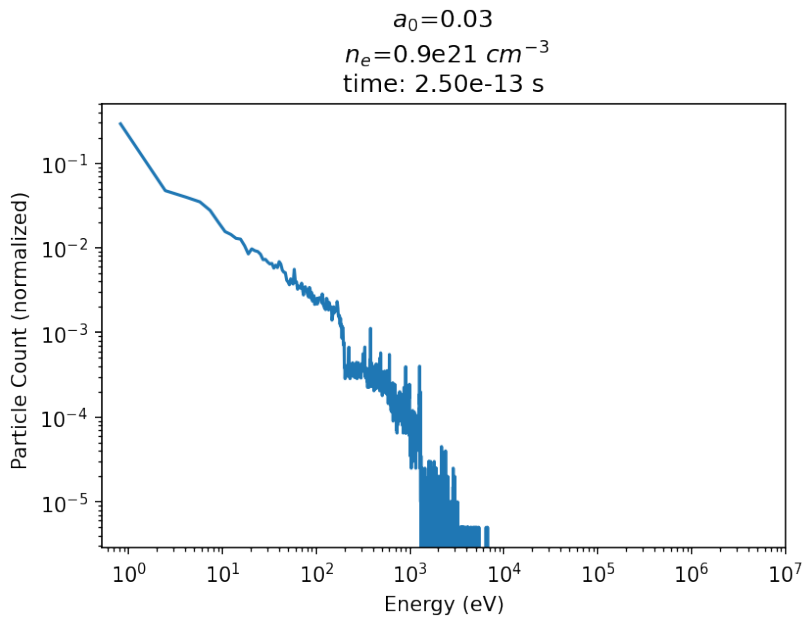

(i)

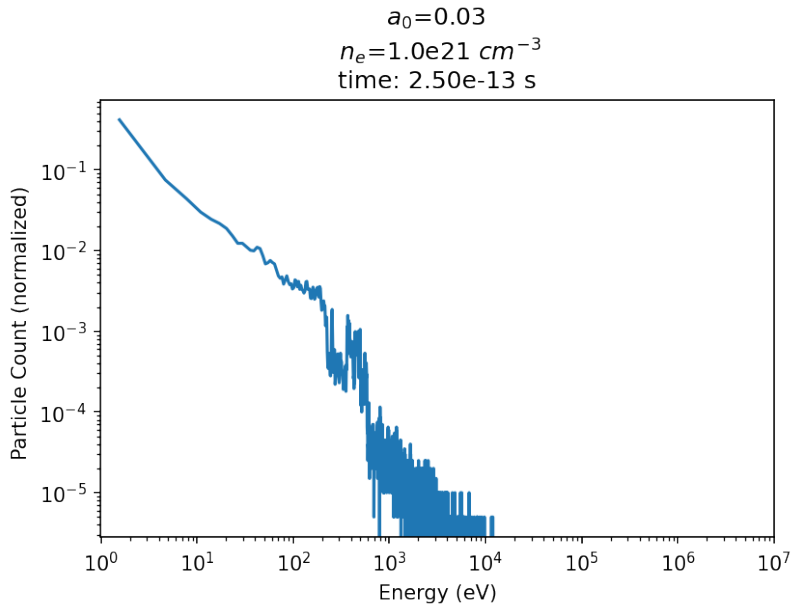

(j)

Fig 3 - Energy distributions at the low intensity of a_0=0.03 show that the maximum energy does not change much for many of the scanned densities. This trend changes once the plasma approaches the high density regime, indicating that perhaps another mechanism occurs which is not present in the low density regime.

From the density range of 0.1e21 cm^{-3} to 0.8e21 cm^{-3}, the maximum electron energy is restricted to approximately 1 keV. However, once the plasma density becomes sufficiently close to the

critical density, the high density acceleration mechanisms, such as sheath acceleration, drive the electrons to higher energies. As such, the 0.9e21cm^{-3} and 1.0e21cm^{-3} cases extend the maximum tail energies from 1 keV to ~10keV. Additionally, the laser intensity is too low to create a wakefield acceleration effect on the electrons, which is why only the high density regime reflects a more substantial energy gain.

For the $a_0 = 0.1$ case, the plasma exhibits LWFA behavior in the low-density regime. However, as shown in Figure 1, the energy gain in the a_0=0.1 case increases with increasing density rather than decreasing. In fact, by examination of the energy curve of conventional LWFA theory, one can see that the electrons of the plasma are actually accelerated to much higher energies than anticipated.While it may seem that LWFA breaks down in this regime, the maximum energy seems to correspond to a new "splash" region in the energy distribution function as shown in Fig 4.

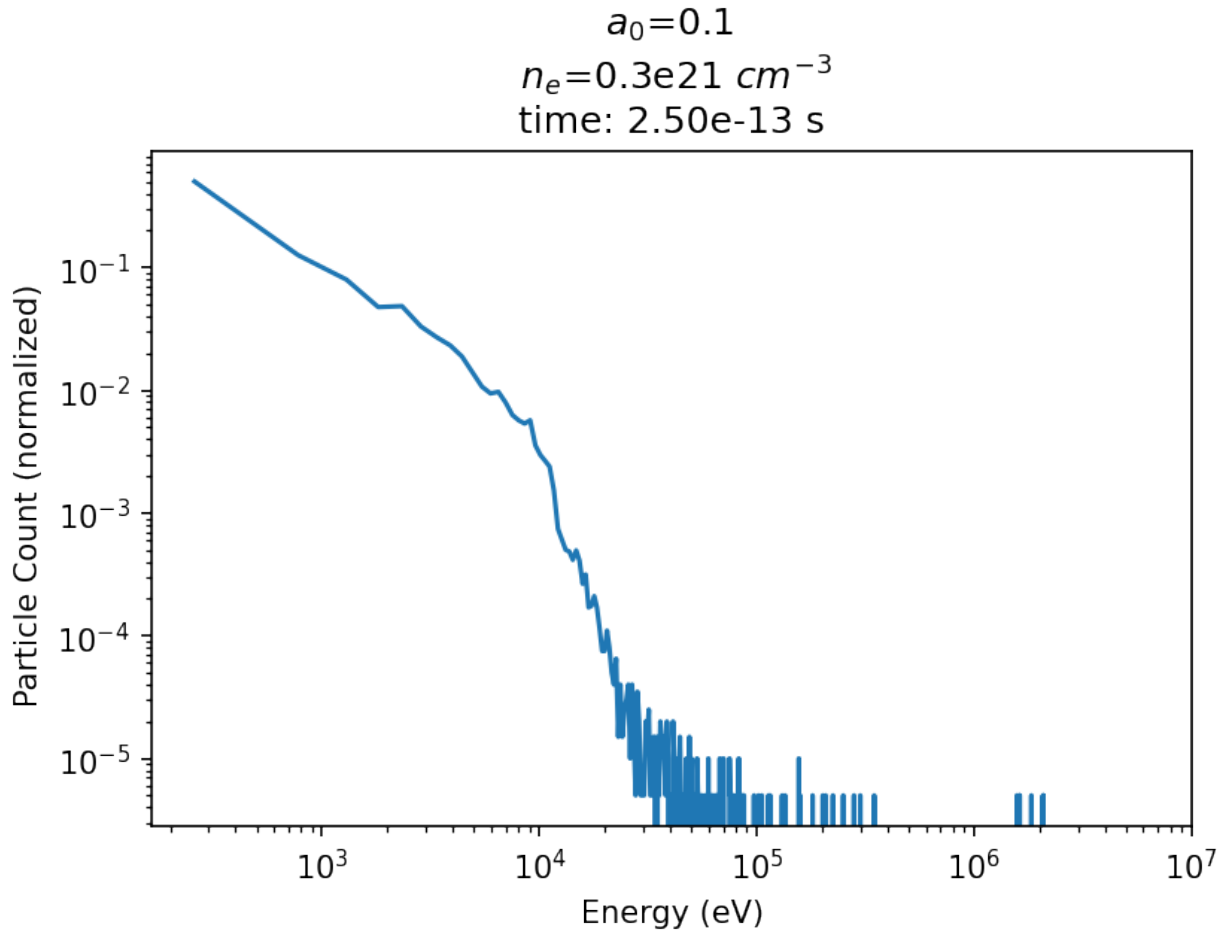

Fig 4 - Energy distribution graphs split into several different sections:

*The bulk wave corresponds to linear portion of function; Falloff corresponds to tail, which ends ~6*10^4 eV; Extension beyond the tail is the "splash" region and has few electrons.*

The energy of the end of the tail region seems to correspond to energy predicted by LWFA theory, whereas the splash reflects another mechanism of acceleration. Additionally, the "splash" region grows as the density approaches the high density region.

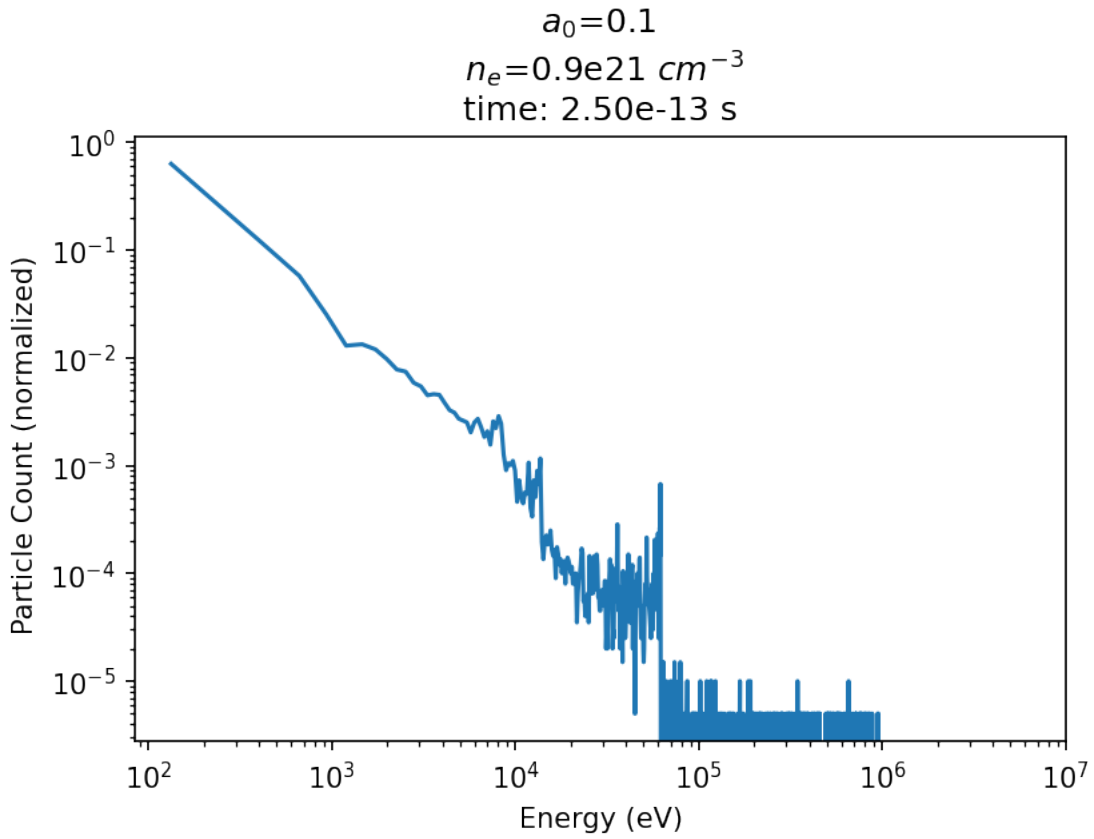

Fig 5 - *The splash region became longer compared to smaller densities, showing more electrons approaching maximum energy of the splash. Additionally, more electrons are accelerated to higher energies in the "tail" region.*

B. High Intensity Laser

In the high intensity regime of a_0=1, the behavior of the maximum energy matches the energy dependence expected from LWFA theory, as shown in Fig 6.

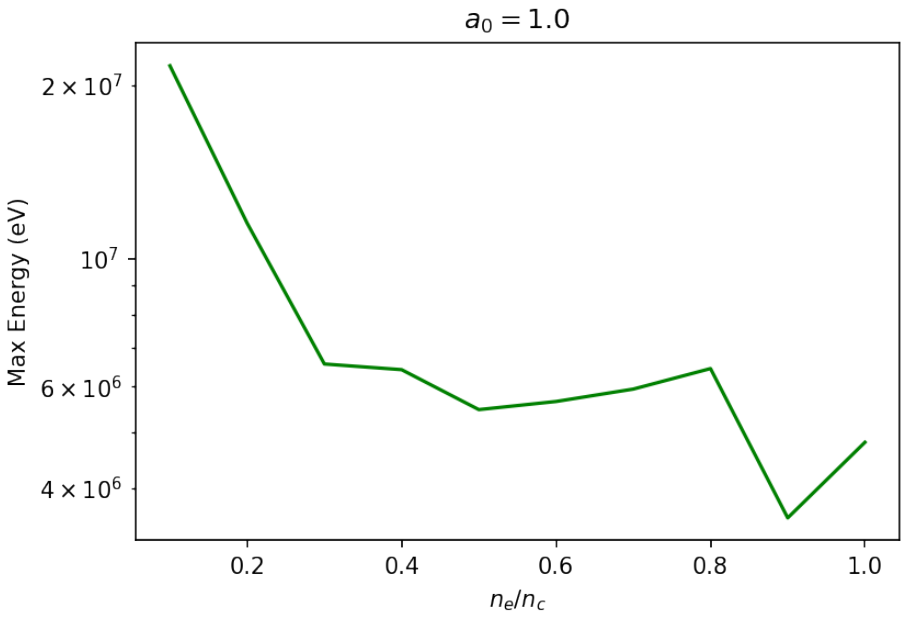

Fig 6 - The energies at all scanned densities generally correspond to LWFA theory in the high intensity regime. For example, energy gain when $n_e=n_{c,}$ is expected to be 4.14 MeV, whereas the energy measured at the critical density is ~5 MeV.

The energy gain begins to follow conventional wakefield predictions at this intensity, where the wakefield energy gain equation predicts the energy gain even at the critical density within one order. However, one can see that there is not a

C. Moderate Intensity Laser

Upon examination of these different results, it is apparent that the intensity determines the primary mechanism of acceleration in the plasma. In other words, it determines whether the maximum energy corresponds or deviates from LWFA theory. Examination of another intensity, a_0=0.3, was completed, as 0.3 is closer to LWFA theory than 0.1, due to higher intensity, but should still have some deviation. As shown in Fig 4, the distribution of the energy

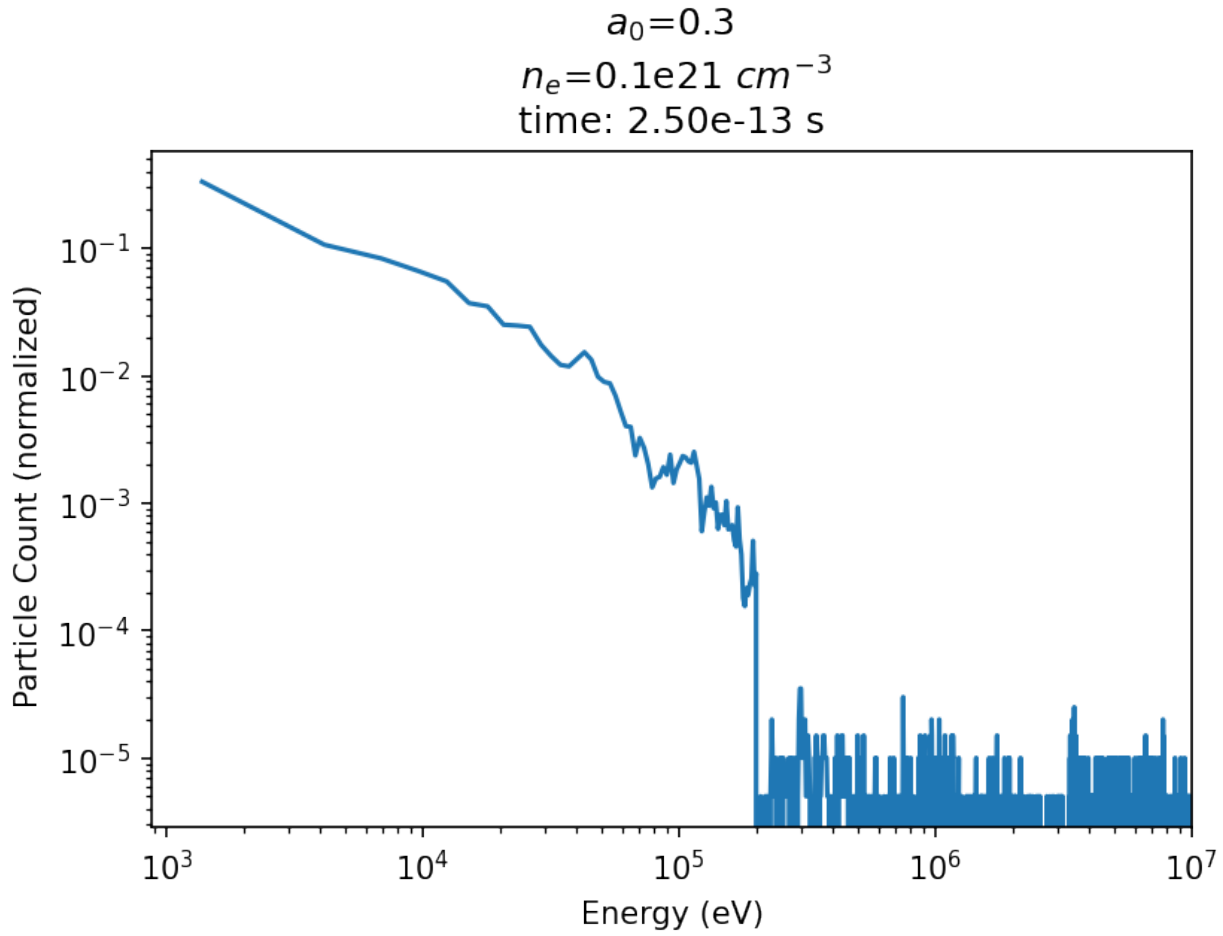
a_0=0.3
n_e=0.1e21 cm^{-3}
time: 2.50e-13 s
Particle Count (normalized)
10^{-1}
10^{-2}
10^{-3}
10^{-4}
10^{-5}
10^3
10^4
10^5
10^6
10^7
Energy (eV)

(a)

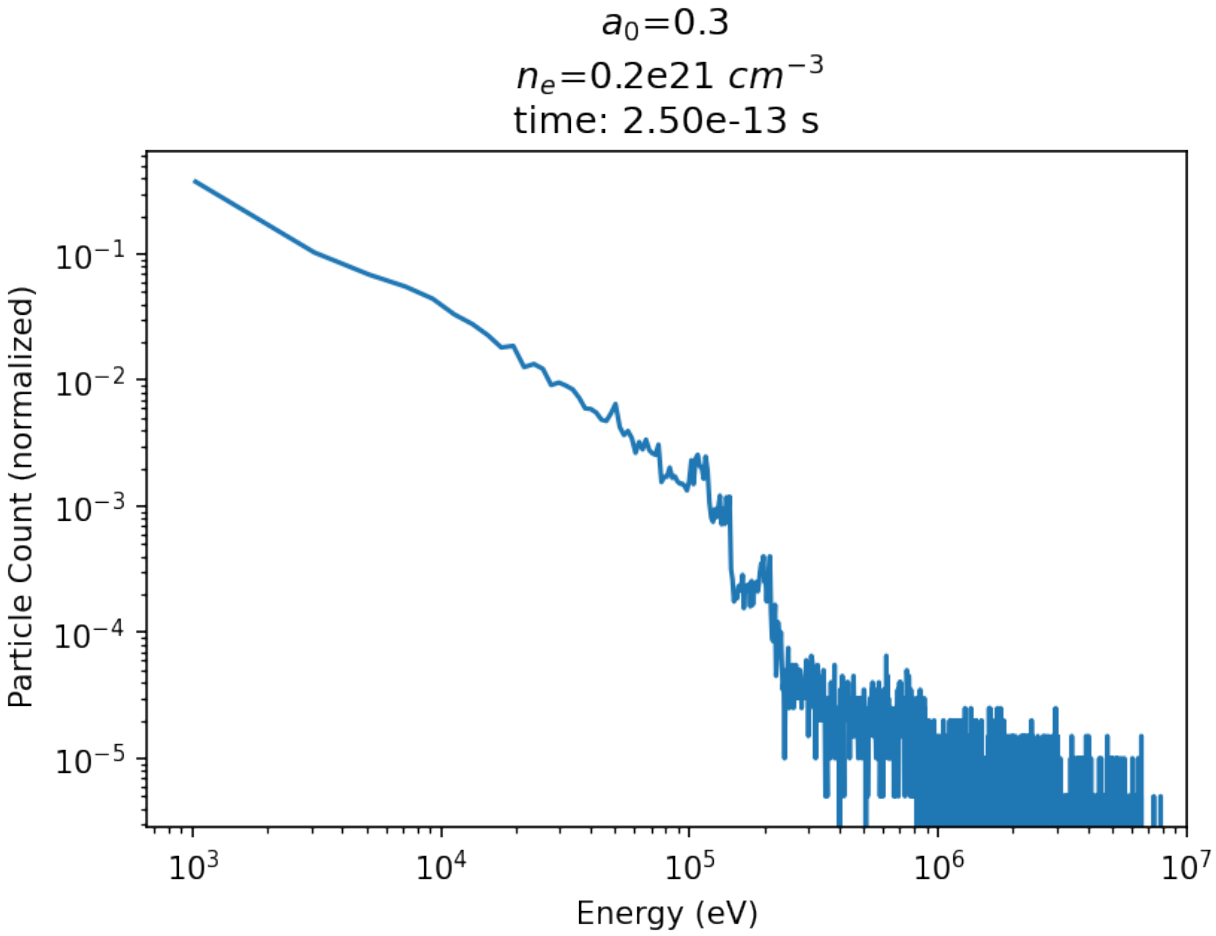
a_0=0.3
n_e=0.2e21 cm^{-3}
time: 2.50e-13 s
Particle Count (normalized)
10^{-1}
10^{-2}
10^{-3}
10^{-4}
10^{-5}
10^3
10^4
10^5
10^6
10^7
Energy (eV)

(b)

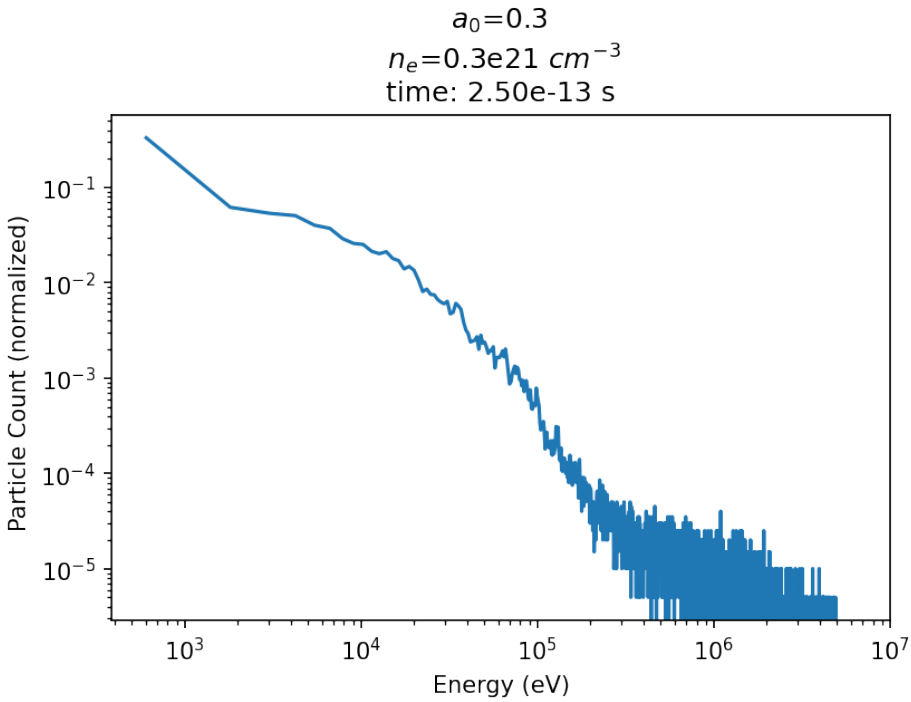
a_0=0.3
n_e=0.3e21 cm^{-3}
time: 2.50e-13 s
Particle Count (normalized)
10^{-1}
10^{-2}
10^{-3}
10^{-4}
10^{-5}
10^3
10^4
10^5
10^6
10^7
Energy (eV)

(c)

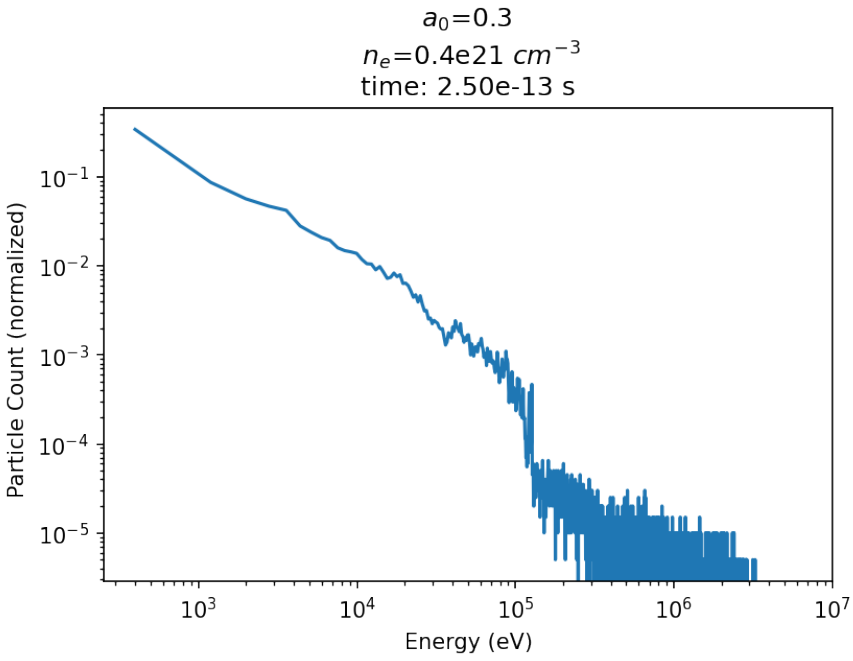
a_0=0.3
n_e=0.4e21 cm^{-3}
time: 2.50e-13 s
Particle Count (normalized)
10^{-1}
10^{-2}
10^{-3}
10^{-4}
10^{-5}
10^3
10^4
10^5
10^6
10^7
Energy (eV)

(d)

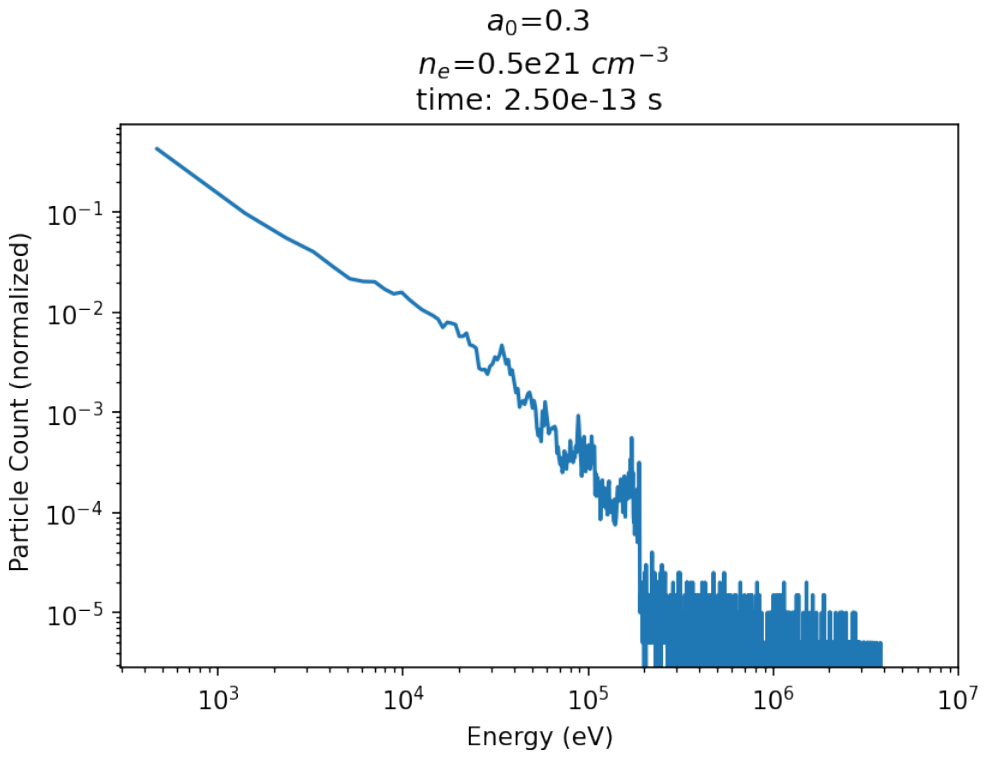
a_0=0.3
n_e=0.5e21 cm^{-3}
time: 2.50e-13 s
Particle Count (normalized)
10^{-1}
10^{-2}
10^{-3}
10^{-4}
10^{-5}
10^3
10^4
10^5
10^6
10^7
Energy (eV)

(e)

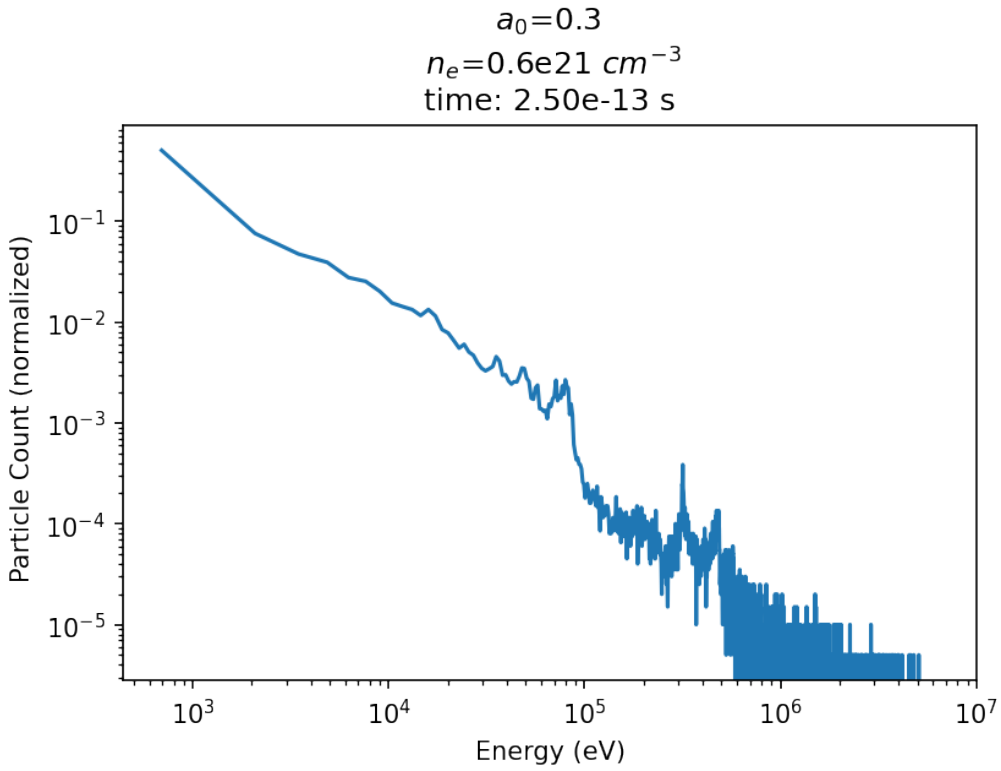
a_0=0.3
n_e=0.6e21 cm^{-3}
time: 2.50e-13 s
Particle Count (normalized)
10^{-1}
10^{-2}
10^{-3}
10^{-4}
10^{-5}
10^3
10^4
10^5
10^6
10^7
Energy (eV)

(f)

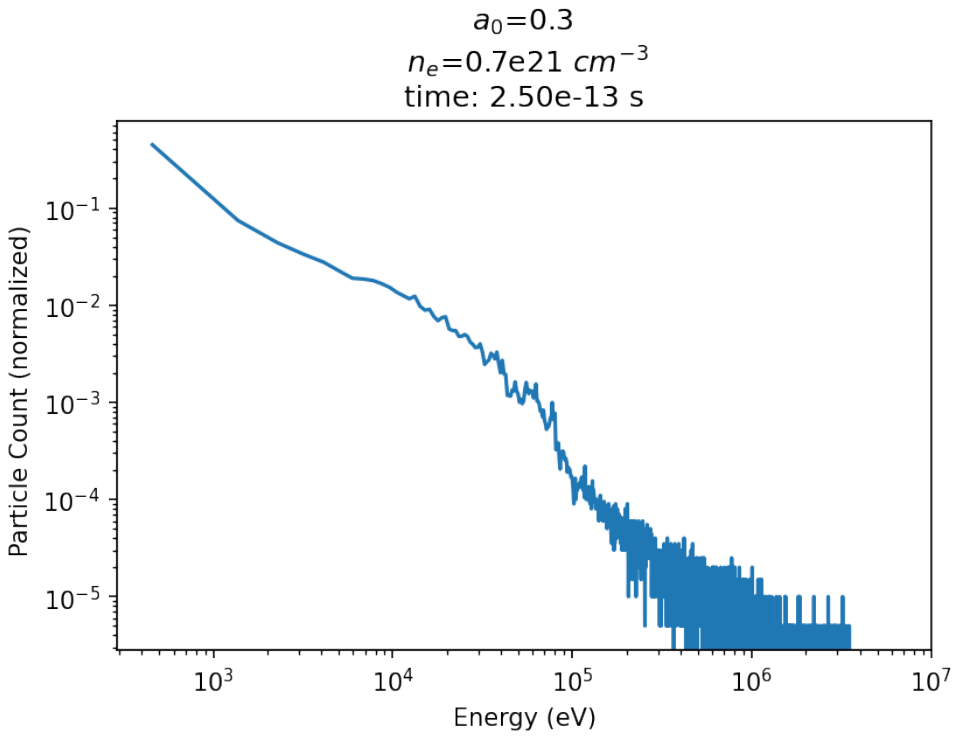
a_0=0.3
n_e=0.7e21 cm^{-3}
time: 2.50e-13 s
Particle Count (normalized)
10^{-1}
10^{-2}
10^{-3}
10^{-4}
10^{-5}
10^3
10^4
10^5
10^6
10^7
Energy (eV)

(g)

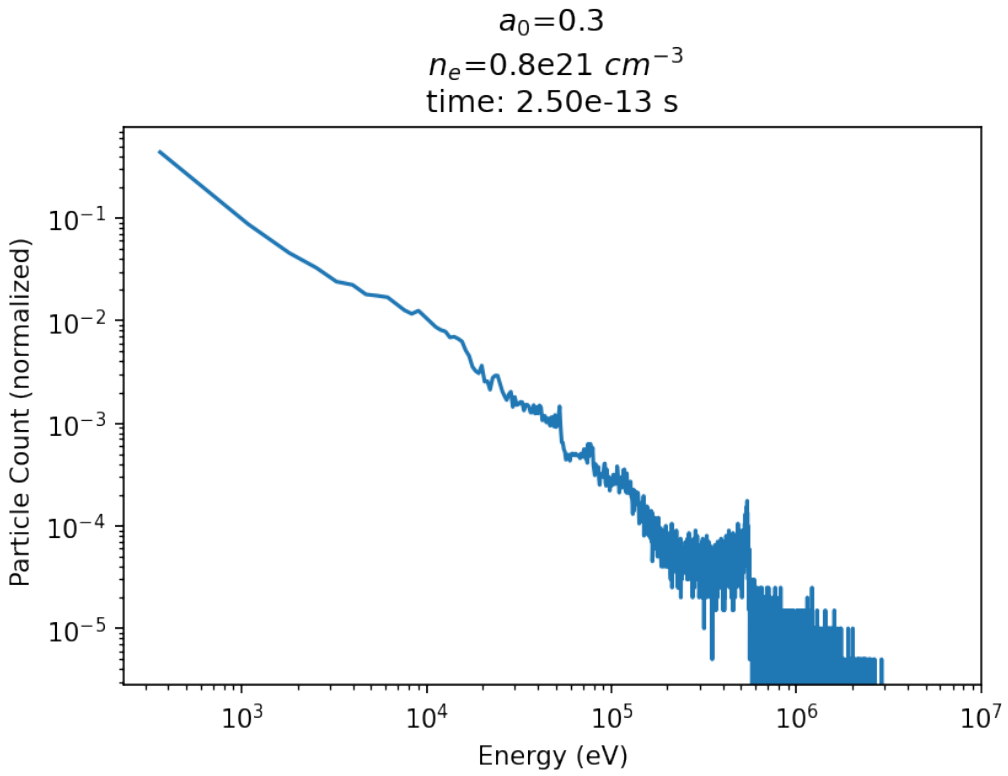
a_0=0.3
n_e=0.8e21 cm^{-3}
time: 2.50e-13 s
Particle Count (normalized)
10^{-1}
10^{-2}
10^{-3}
10^{-4}
10^{-5}
10^3
10^4
10^5
10^6
10^7
Energy (eV)

(h)

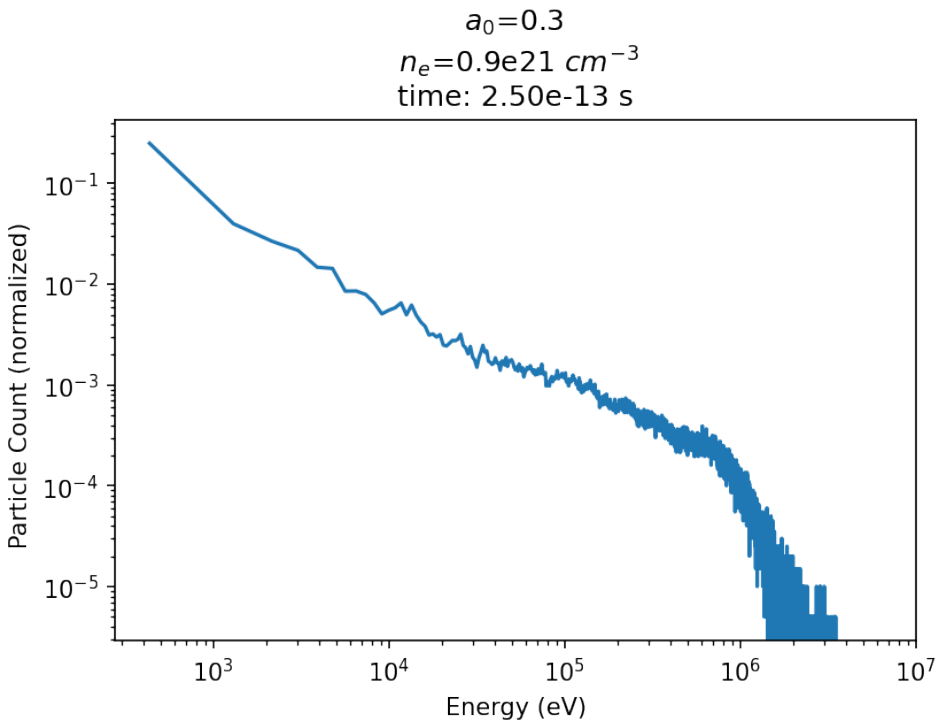
a_0=0.3
n_e=0.9e21 cm^{-3}
time: 2.50e-13 s
Particle Count (normalized)
10^{-1}
10^{-2}
10^{-3}
10^{-4}
10^{-5}
10^3
10^4
10^5
10^6
10^7
Energy (eV)

(i)

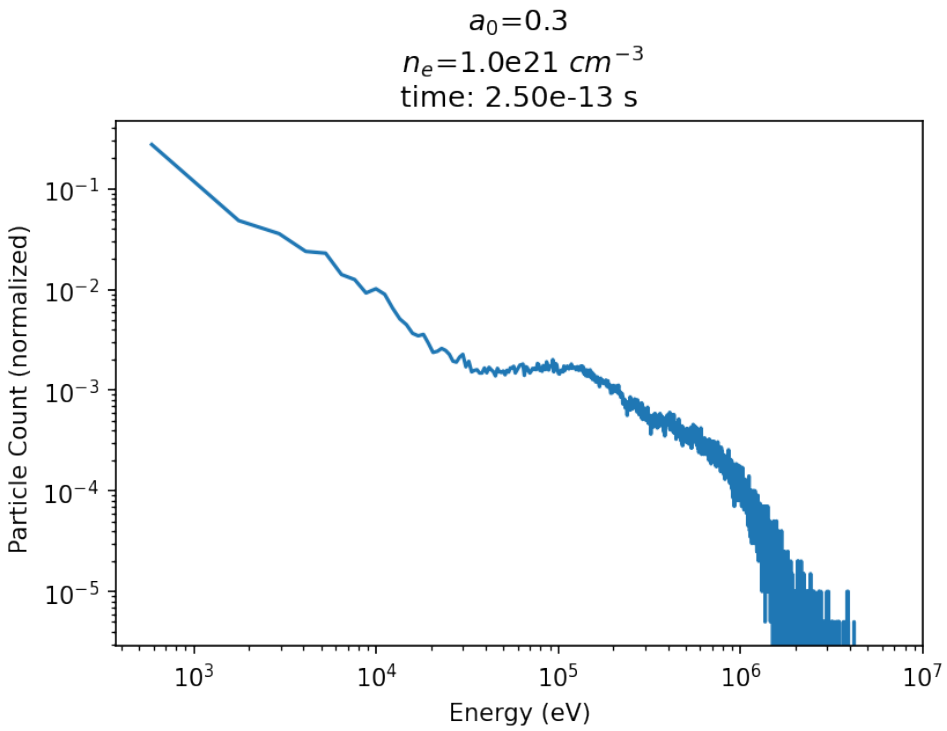
a_0=0.3
n_e=1.0e21 cm^{-3}
time: 2.50e-13 s
Particle Count (normalized)
10^{-1}
10^{-2}
10^{-3}
10^{-4}
10^{-5}
10^3
10^4
10^5
10^6
10^7
Energy (eV)

(j)

Fig 7 - The highest energy value corresponds to the "splash" region rather than the end of the tail region. However, the splash region becomes less pronounced as the plasma density approaches the critical density.

shows the maximum energy reached by the electrons and the LWFA energy prediction comes from the "splash" of the plasma rather than the tail. However, the energy does exhibit a relationship closer to the inversely proportional relationship with the plasma density predicted by LWFA theory, as shown in figure 8.

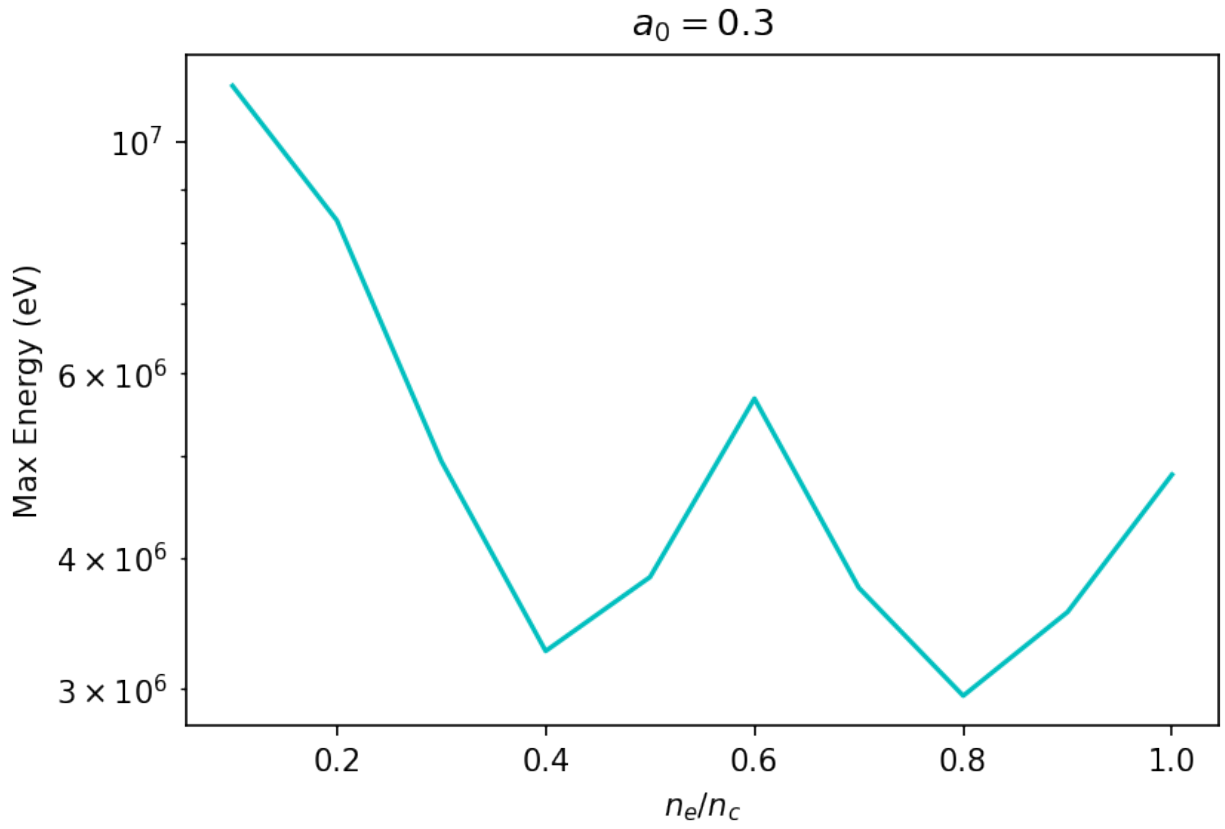

Fig 8 - Maximum energy plotted against the density ratio shows that the maximum energy at lower densities represent a close match to LWFA predictions. Eventually, the maximum energy increases towards the critical density.

As such, conventional LWFA theory seems to offer pieces of the puzzle at the mid-intensity simulation of a_0=0.3. The maximum energy drops with density from n_e/n_c=0.1 to 0.4, reflecting the inverse relationship the energy gain has with n_e according to LWFA theory. However, the energy values rise from n_e/n_c=0.4 to 0.6 and 0.8 to 1.0, showing once more a departure from conventional LWFA theory. Additionally, the splash region noticeably shrinks and the tail region

grows taller as the density approaches n_c. This shows that a large portion of electrons are being accelerated to similar energies close to the maximum energy. In contrast, the low density cases, such as $n_e/n_c=0.1$, have wide splash and short tail regions from which the maximum energy is measured.

Chapter 3 -

I. Conclusion

Through particle-in-cell simulation, we have found that extremely low intensities, such as a_0=0.03, require explanations supplemental to known LWFA predictions but show promise in accelerating electrons to low energies. Low intensity laser pulses do not seem to allow electrons to reach the often desired high energy electrons attainable by the well-studied low density, high intensity regime of LWFA. This is not a major issue and is, in fact, the goal in mind for this study; ideally, a bulk of ~100keV electrons are created rather than high MeV or even GeV electrons. The additional usage of a beat wave rather than a single pulse counteracts the long pulse width limitation of fiber lasers, as the beat wave can still create a wave at the plasma frequency. When a_0 increased from 0.03, the bulk of the plasma was able to reach the 100 keV energies without requiring lasers close to a_0=1. In fact, the maximum energy of the electrons in these intermediary intensities were found to be higher than that predicted by typical LWFA theory as the plasma target approached the critical density, showing that this high density mechanism plays an additional role in accelerating electrons once the density becomes large enough. While the simulation can be refined, such as through the introduction of spatial boundaries or implementation of a specific plasma target, the results both answer and lead into new questions for LWFA in the high density regime.

II. Acknowledgements

This work was supervised closely by Ernesto Barraza and Professor Toshiki Tajima, without whom much of this work would be done without analysis and understanding. Professor Tajima patiently guided me through proper steps of research and reminded me to open my eyes and let mother nature speak. Ernesto Barraza always engaged in discussion with me even on small questions I had and helped me gain confidence in my own ability to understand and work.
I would also like to acknowledge Dr. Scott Nicks, who laid the groundwork for this research with one of the first ventures into the high-density regime and provided code to analyze the phase space in python, and Professor Zhihong Lin, who taught the UCI plasma physics course, which was my first official course in the field. It is no understatement to say this work represents the culmination of support and mentorship I have received during my time at UCI.

References:

[1] T. Tajima, K. Nakajima, and G. Mourou, *Laser acceleration*, La Rivista del Nuovo Cimento 40, 33 (2017).

[2] T. Tajima and J. M. Dawson, *Laser electron accelerator*, Phys. Rev. Lett. 43, 267 (1979).

[3] Tajima, T., *Plasma-fiber Laser Accelerator*, Proc. Laser 1983 (1984) p. 104.

[4] Tajima, T., *High Energy Laser Plasma Accelerators*, Laser and Particle Beams **3**, 351 (1985).

[5] D. Strickland and G. Mourou, *Compression of amplified chirped optical pulses*, Opt. Commun. 56, 219 (1985).

[6] K. Nakajima et al., *Laser wakefield accelerator experiments using 1 ps 30 TW Nd*:glass laser, in Proceedings of International Conference on Particle Accelerators, Vol. 4 (IEEE, Washington, DC, 1993) pp. 2556–2558.

[7] K. Nakajima et al., *A proof-of-principle experiment of laser wakefield acceleration*, Phys. Scr. T52, 61 (1994).

[8] E. Fourkal, B. Shahine, M. Ding, J. S. Li, T. Tajima, and C.-M. Ma, *Particle in cell simulation of laser-accelerated proton beams for radiation therapy*, Med. Phys. 29, 2788 (2002).

[9] W. Newhauser and R. Zhang, *The physics of proton therapy,* Phys. Med. Biol. 60, R155 (2015).

[10] S. V. Bulanov, H. Daido, T. Z. Esirkepov, V. S. Khoroshkov, J. Koga, K. Nishihara, F. Pegoraro, T. Tajima, and M. Yamagiwa, *Feasibility of using laser ion accelerators in proton therapy*, AIP Conf. Proc. 740, 414 (2004).

[11] T. Tajima, P*rospect for compact medical laser accelerators,* J. Jpn. Soc. Therp. Radiat. Oncol. 9, 83 (1997).

[12] C. Chiu, M. Fomytskyi, F. Grigsby, F. Raischel, M. C. Downer, and T. Tajima, *Laser electron accelerators for radiation medicine: A feasibility study*, Med. Phys. 31, 2042 (2004).

[13] K. K. Kainz, K. R. Hogstrom, J. A. Antolak, P. R. Almond, C. D. Bloch, C. Chiu, M. Fomytskyi, F. Raischel, M. Downer, and T. Tajima, *Dose properties of a laser accelerated electron beam and prospects for clinical application*, Med. Phys. 31, 2053 (2004).
[14] A. Giulietti, N. Bourgeois, T. Ceccotti, X. Davoine, S. Dobosz, P. D'Oliveira, M. Galimberti, J. Galy, A. Gamucci, et al., *Intense γ-ray source in the giant dipole-resonance range driven by 10-TW laser pulses*, Phys. Rev. Lett. 101, 105002 (2008).
[15] A. Giulietti, ed., *Laser-Driven Particle Acceleration Towards Radiobiology and Medicine* (Springer International Publishing, Switzerland, 2016).15
[16] K. Nakajima, J. Yuan, L. Chen, and Z. Sheng, *Laserdriven very high energy electron/photon beam radiation therapy in conjunction with a robotic system*, Applied Sciences 5, 1 (2015).
[17] K. Nakajima, *Laser-driven electron beam and radiation sources for basic, medical and industrial sciences,* Proceedings of the Japan Academy, Series B 91, 223 (2015).
[18] G. Mourou, W. Brocklesby, T. Tajima, and J. Limpert, The future is fibre accelerators, Nat. Photonics 7, 258 (2013).
[19] B. S. Nicks, T. Tajima, D. Roa, A. Neˇcas, and G. Mourou, *Laser-wakefield application to oncology*, Int. J. Mod. Phys. A 34, 1943016 (2019).
[20] S. C. Wilks, W. L. Kruer, M. Tabak, and A. B. Langdon, *Absorption of ultra-intense laser pulses*, Phys. Rev. Lett. 69, 1383 (1992).
[21] P. Valenta, O. Klimo, G. M. Grittani, T. Z. Esirkepov, G. Korn, and S. V. Bulanov, *Wakefield excited by ultrashort laser pulses in near-critical density plasmas*, in Laser Acceleration of Electrons, Protons, and Ions V , Vol. 11037, edited by E. Esarey, C. B. Schroeder, and J. Schreiber, International Society for Optics and Photonics (SPIE, 2019) pp. 57 – 65.
[22] T. O'Neil, *Collisionless damping of nonlinear plasma oscillations*, Phys. Fluids 8, 2255 (1965).
[23] F. Mako and T. Tajima, C*ollective ion acceleration by a reflexing electron beam: Model and scaling*, Phys. Fluids 27, 1815 (1984).
[24] H. Lamb, in Hydrodynamics (Dover Publications, New York, 1945) Chap. 8.

[25] A. Pukhov and J. Meyer-ter-Vehn, *Relativistic magnetic self-channeling of light in near-critical plasma: Three Dimensional particle-in-cell simulation,* Phys. Rev. Lett. 76, 3975 (1996).

[26] F. Sylla, A. Flacco, S. Kahaly, M. Veltcheva, A. Lifschitz, V. Malka, E. d'Humieres, I. Andriyash, and V. Tikhonchuk, *Short intense laser pulse collapse in near-critical plasma*, Phys. Rev. Lett. 110, 085001 (2013).

[27] Chattopadyay, S., Mourou, G., Shiltsev, V., and Tajima, T., Editors, *Beam acceleration in Crystals and Nanostructures* (World scientific, Singapore, 2020).

[28] T. Tajima, X. Q. Yan, and T. Ebisuzaki, *Wakefield acceleration,* Rev. Modern Plasma Phys. **4,** 7 (2020). https://link.springer.com/article/10.1007/s41614-020-0043-z

[29] B.S. Nicks, S. Hakimi, E. Barraza-Valdez, K.D. Chestnut, G.H. DeGrandchamp, K.R. Gage, D. B. Housley, G. Huxtable, G. Lawler, D.J. Lin, P. Manwani, E.C. Nelson, G.M. Player, M.W.L. Seggebruch, J. Sweeney, J.E. Tanner, K. Thompson, and T. Tajima, *Electron Dynamics in the High-Density Laser-Wakefield Acceleration Regime,* to be published in Photonics (2021).

[30] M. C. Downer, et al., Rev. Mod. Phys. **90**, 035002 (2018).

[31] D. M. Farinella, J. Wheeler, A. Hussein, J. Nees, M. Stanfield N. Beier, G. Cojocaru, G. Ungureanu, M. Pittman, J. Demailly, E. Baynard, R. Fabbri, R. Secareanu, M. Masruri, A. Maksimchuk, K. Krushelnick, G. Mourou, T. Tajima, and F. J. Dollar, *Focusability of high intensity laser pulses after self-phase modulation in thin films,* J. Opt. Soc. Am. B **36,** 000A28 (2019).